Multidimensional Langevin Modeling of Nonoverdamped Dynamics

Norbert Schaudinnus,[1] Björn Bastian,[1] Rainer Hegger,[2] and Gerhard Stock[1,*]
[1]Biomolecular Dynamics, Institute of Physics, Albert Ludwigs University, 79104 Freiburg, Germany
[2]Institute of Physical and Theoretical Chemistry, Goethe University, 60438 Frankfurt, Germany
(Received 30 March 2015; published 30 July 2015)

Based on a given time series, data-driven Langevin modeling aims to construct a low-dimensional dynamical model of the underlying system. When dealing with physical data as provided by, e.g., all-atom molecular dynamics simulations, effects due to small damping may be important to correctly describe the statistics (e.g., the energy landscape) and the dynamics (e.g., transition times). To include these effects in a dynamical model, an algorithm that propagates a second-order Langevin scheme is derived, which facilitates the treatment of multidimensional data. Adopting extensive molecular dynamics simulations of a peptide helix, a five-dimensional model is constructed that successfully forecasts the complex structural dynamics of the system. Neglect of small damping effects, on the other hand, is shown to lead to significant errors and inconsistencies.

DOI: 10.1103/PhysRevLett.115.050602 PACS numbers: 05.10.-a, 05.20.Gg, 87.15.-v

Time series analysis is used in many areas to construct a dynamical model of the behavior of some complex systems [1]. Given a (in general multidimensional) time series $\boldsymbol{x}(t)$, for example, a popular approach is to partition $\boldsymbol{x}(t)$ in discrete metastable states such that there is a time scale separation between fast intrastate fluctuations and slow interstate transitions. By constructing the corresponding transition matrix, we obtain a Markov state model [2], which approximates the dynamics of the system by a memoryless jump process. Alternatively, we may assume that $\boldsymbol{x}(t)$ can be described by a Langevin equation [3]

$$\dot{\boldsymbol{x}}(t) = \boldsymbol{h}(\boldsymbol{x}) + \mathcal{D}(\boldsymbol{x})\boldsymbol{\xi}(t), \tag{1}$$

where $\boldsymbol{h}(\boldsymbol{x})$ is the deterministic drift field of the dynamics and $\mathcal{D}(\boldsymbol{x})\boldsymbol{\xi}(t)$ describes the stochastic driving of the system. The latter consists of the diffusion field $\mathcal{D}(\boldsymbol{x})$ and the "noise" $\boldsymbol{\xi}(t)$, which usually is assumed to be of zero mean, $\langle\boldsymbol{\xi}\rangle = \boldsymbol{0}$, delta correlated, $\langle\xi_i(t)\xi_j(t')\rangle = \delta_{ij}\delta(t-t')$, and Gaussian distributed. Given a time series $\boldsymbol{x}(t)$, the basic idea of data-driven Langevin equation (dLE) modeling is to determine the Langevin fields $\boldsymbol{h}$ and $\mathcal{D}$, which together with the properties of the noise constitute the desired dynamical model. The model can then be employed to forecast the essential statistical and dynamical features of the original time series, to predict the system's long-time behavior from many (but short) pieces of input data, and for interpretation purposes [4–10].

To assess the validity of a Langevin model, it is instructive to consider its underlying approximations. Using projection techniques, Zwanzig derived an exact generalized Langevin equation that includes a memory kernel, which describes the non-Markovian coupling of the system to the environment [11]. When we assume a time scale separation between the slow system coordinate $\boldsymbol{x}$ and the remaining fast bath coordinates (i.e., a Markov approximation), we obtain a second-order Langevin equation

$$\ddot{\boldsymbol{x}}(t) = \boldsymbol{f}(\boldsymbol{x}) - \Gamma(\boldsymbol{x})\dot{\boldsymbol{x}} + \mathcal{K}(\boldsymbol{x})\boldsymbol{\xi}(t), \tag{2}$$

which contains a Newtonian force term $\boldsymbol{f}(\boldsymbol{x})$, a Stokes' friction term $\Gamma(\boldsymbol{x})\dot{\boldsymbol{x}}$, and a stochastic force $\mathcal{K}(\boldsymbol{x})\boldsymbol{\xi}(t)$. Assuming furthermore that inertial effects causing the acceleration $\ddot{\boldsymbol{x}}$ can be neglected, we finally arrive at the first-order equation (1) that accounts for overdamped motion. Hence, a data-driven model using Eq. (1) can only correctly account for the dynamics of $\boldsymbol{x}(t)$ if a clear system-bath time scale separation exists and if the dynamics is overdamped. Otherwise, we may not obtain a consistent dynamical model that correctly reproduces the statistics and dynamics of the input data and satisfies as well the implied assumptions on the noise.

As a prime application, the above described approach has been employed to model classical molecular dynamics (MD) simulations [4–10]. Using a systematic dimensionality reduction method (see below), one can always enforce a system-bath time scale separation at the expense of a higher dimension of the reaction coordinate. On the other hand, it clearly depends on the system and simulation conditions or even on the details of the data preprocessing, whether the resulting dynamics described by $\boldsymbol{x}(t)$ appears to be overdamped or not. Notwithstanding its potential importance, to our knowledge no practical method to propagate a multidimensional second-order dLE (dLE2) exists, while several schemes have been proposed in the first-order case [5–9] (dLE1). In this work we therefore develop an approach to construct a dLE2 and demonstrate the performance of the method and the importance of small damping effects by forecasting the five-dimensional structural dynamics of a peptide helix [12].

When we work with simulated or measured data, we typically have a discrete time series $\boldsymbol{x}_n \equiv \boldsymbol{x}(n\Delta t)$, where Δt denotes the time step of the data, which we set to $\Delta t \equiv 1$ for notational convenience. As a consequence, the time derivatives of the dLE2 in Eq. (2) are approximated by finite differences. This leads to the time discrete equations of motion

$$\boldsymbol{x}_{n+1} = \boldsymbol{x}_n + \boldsymbol{f}(\boldsymbol{x}_n) - \hat{\Gamma}(\boldsymbol{x}_n)\boldsymbol{v}_n + \mathcal{K}(\boldsymbol{x}_n)\boldsymbol{\xi}_n, \tag{3}$$

where $\hat{\Gamma} = \Gamma - \mathbb{I}$, $\boldsymbol{\xi}_n = \boldsymbol{\xi}(t_n)$, and $\boldsymbol{v}_n = \boldsymbol{x}_n - \boldsymbol{x}_{n-1}$ denotes the velocity. We note that for $\hat{\Gamma} = 0$, the dLE2 reduces to a dLE1.

Because the noise term $\boldsymbol{\xi}$ is not known, the fields $\boldsymbol{f}(\boldsymbol{x}_n)$, $\hat{\Gamma}(\boldsymbol{x}_n)$, and $\mathcal{K}(\boldsymbol{x}_n)$ cannot be obtained directly (e.g., via a least squares fit) from the input data, but need to be calculated by invoking some coordinate-dependent statistical average over the noise [9]. To define a local average $\langle F(\boldsymbol{x})\rangle$ of the quantity F over the neighborhood of a given point $\boldsymbol{x}_n$, we distinguish two cases. If the function F is evaluated at reference point $\boldsymbol{x}_n$, the local average can be approximated by $F(\boldsymbol{x}_n)$, i.e., the function evaluated at $\boldsymbol{x}_n$. This holds since by construction the fluctuations of the neighboring points are small. For the dLE2 in Eq. (3), this applies to the Langevin fields $\boldsymbol{f}(\boldsymbol{x}_n)$, $\hat{\Gamma}(\boldsymbol{x}_n)$, and $\mathcal{K}(\boldsymbol{x}_n)$ as well as for $\boldsymbol{x}_n$ itself. On the other hand, the temporal predecessors and successors of the neighbors of $\boldsymbol{x}_n$ may show large fluctuations due to different velocities and the stochastic force. To calculate a local average over these points, we define

$$\langle \boldsymbol{x}_{n\pm1}\rangle = \frac{1}{k}\sum_i \boldsymbol{x}_{i\pm1}\Theta(|\boldsymbol{x}_i - \boldsymbol{x}_n| - \epsilon_k), \tag{4}$$

where the sum goes over the k nearest neighbors of reference point $\boldsymbol{x}_n$. The Heaviside step function Θ ensures that only points within a distance ϵ_k are considered, where $\epsilon_k(\boldsymbol{x}_n)$ is locally chosen such that exactly k neighbors contribute. That is, when a function F depends on the predecessors $\boldsymbol{x}_{i-1}$ or successors $\boldsymbol{x}_{i+1}$, we average F over all neighbor indices i.

To calculate the Langevin fields $\boldsymbol{f}_n = \boldsymbol{f}(\boldsymbol{x}_n)$, $\hat{\Gamma}_n = \hat{\Gamma}(\boldsymbol{x}_n)$, and $\mathcal{K}_n = \mathcal{K}(\boldsymbol{x}_n)$, we perform the above defined local average on both sides of Eq. (3), which yields

$$\langle \boldsymbol{x}_{n+1}\rangle = \boldsymbol{x}_n + \boldsymbol{f}_n - \hat{\Gamma}_n(\boldsymbol{x}_n - \langle \boldsymbol{x}_{n-1}\rangle), \tag{5}$$

where we used that $\langle\boldsymbol{\xi}\rangle = \boldsymbol{0}$. Similarly, we consider

$$\langle \boldsymbol{x}_{n+1}\boldsymbol{x}_{n-1}^T\rangle = (\boldsymbol{x}_n + \boldsymbol{f}_n)\langle \boldsymbol{x}_{n-1}^T\rangle - \hat{\Gamma}_n(\boldsymbol{x}_n\langle \boldsymbol{x}_{n-1}^T\rangle - \langle \boldsymbol{x}_{n-1}\boldsymbol{x}_{n-1}^T\rangle). \tag{6}$$

Combining these equations, we obtain the desired dLE2 fields

$$\hat{\Gamma}_n = \mathcal{C}(\boldsymbol{x}_{n+1}, \boldsymbol{x}_{n-1})\mathcal{C}^{-1}(\boldsymbol{x}_{n-1}, \boldsymbol{x}_{n-1}), \tag{7}$$

$$\boldsymbol{f}_n = \langle \boldsymbol{x}_{n+1}\rangle - \boldsymbol{x}_n + \hat{\Gamma}_n(\boldsymbol{x}_n - \langle \boldsymbol{x}_{n-1}\rangle), \tag{8}$$

$$\mathcal{K}_n\mathcal{K}_n^T = \mathcal{C}(\boldsymbol{x}_{n+1}, \boldsymbol{x}_{n+1}) - \hat{\Gamma}_n\mathcal{C}(\boldsymbol{x}_{n-1}, \boldsymbol{x}_{n+1}), \tag{9}$$

where $\mathcal{C}(\boldsymbol{x}, \boldsymbol{y}) = \langle \boldsymbol{x}\boldsymbol{y}^T\rangle - \langle \boldsymbol{x}\rangle\langle \boldsymbol{y}^T\rangle$. Finally, the diffusion matrix $\mathcal{K}$ is calculated from $\mathcal{K}\mathcal{K}^T$ via a Cholesky decomposition [13].

To illustrate the algorithm introduced above, we consider the peptide helix Aib_9 as a simple biomolecular system that nonetheless exhibits complex structural dynamics [12]. The complexity arises from a "hierarchical" free energy landscape of the system [14–17], which reflects dynamical processes on several time scales. They correspond to chiral left- to right-handed transitions of the entire peptide helix that happen on a microsecond time scale, conformational transitions of individual residues, which take about 1 ns, and the opening and closing of structure-stabilizing hydrogen bonds, which occur within tens of picoseconds and are triggered by subpicosecond structural fluctuations. As detailed in Ref. [12], we performed extensive (8×2 μs) MD simulations of Aib_9 in explicit chloroform solvent at 320 K, using the GROMACS program suite [18].

To construct a low-dimensional system coordinate $\boldsymbol{x} = \{x_i\}$ from the high-dimensional MD data, we performed a principal component analysis (PCA), which is a linear transformation that diagonalizes the covariance matrix [19–22]. To this end, we extracted from the MD trajectory the backbone dihedral angles $\phi_n(t)$ and $\psi_n(t)$ of the inner residues ($n = 3, \ldots, 7$) of Aib_9. Ordering the eigenvalues of the resulting dihedral angle PCA [23] decreasingly, it has been shown that a large part of the fluctuations of a molecular system can be represented by the first few principal components (PCs) $x_i(t)$, which usually also account for the slowest motion of the system. Showing the autocorrelation functions $C_i(t) = \langle \delta x_i(t)\delta x_i(0)\rangle / \langle \delta x_i^2\rangle$ ($\delta x_i = x_i - \langle x_i\rangle$) of the first ten PCs, Fig. 1(a) indeed

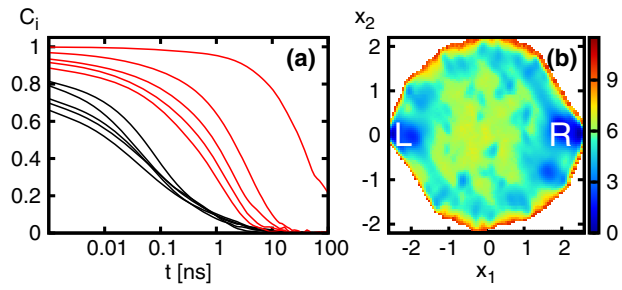

FIG. 1 (color online). (a) Autocorrelation functions of the first ten PCs of Aib_9, revealing a clear time scale separation between slow system coordinates $x_1, \ldots, x_5$ (red) and fast bath coordinates $x_i(t)$ ($i \geq 6$, black). (b) Two-dimensional representation $F(x_1, x_2)$ of the free energy landscape (in units of $k_\mathrm{B}T$) of Aib_9 along the first two PCs.

reveals that the first PC of Aib_9 decays within ≈100 ns and the next four PCs within some nanoseconds, while all higher PCs decay much faster. Hence, to achieve a time scale separation between slow system coordinates (the first few PCs) and fast bath coordinates (all higher PCs), we could include either one or five PCs into a dynamical model.

To decide on this issue, we consider free energy landscapes of Aib_9, e.g., $F(x_1, x_2) = -k_B T \ln P(x_1, x_2)$, where $P(x_1, x_2)$ denotes the probability distribution along the first two PCs [Fig. 1(b)]. Because of the achirality of Aib, we find an overall symmetry with respect to x_1, where the two main minima correspond to the all left-handed structure L and the all right-handed structure R. Moreover, a number of metastable intermediate states can be observed, indicating that an appropriate model of the dynamics needs to include (at least) these two coordinates. In line with the above discussion on the time scale separation, a closer analysis [12] indeed shows that five PCs are required to clearly resolve the metastable conformational states. Hence, we end up with a five-dimensional dLE model of the structural dynamics of Aib_9. We calculate the Langevin fields in Eqs. (7)–(9) locally and "on the fly" (i.e., at every propagation step of the dLE) by using a box-assisted algorithm [13], because the calculation of (more than one-dimensional) global fields of a stochastic differential equation is rather cumbersome.

Employing the MD time series of the system coordinate $\boldsymbol{x}(t)$ as input data, we are now in a position to construct a dLE model of the dynamics of Aib_9. Using a time step of $\Delta t = 1$ ps to resolve the picosecond dynamics of the system, we obtain 1.6×10^7 input points, which are reduced to 10^6 points by using the pruning algorithm described in Ref. [13]. Moreover, we chose $k = 300$ neighbor points to evaluate the local average according to Eq. (4) and integrated the dLE2 in Eq. (3) for 10×2 μs. As a first test of the performance of the Langevin model, Fig. 2 shows the autocorrelation functions and the free energy curves pertaining to the first three PCs. Compared are the MD reference data, the results of the dLE2, as well as the results of a dLE1 whose implementation was introduced previously [13]. Most notably, we find that the dLE2 reproduces the decay of the autocorrelations excellently, while the dLE1 predicts decays that are more than 1 order of magnitude faster. Similarly, the free energy curves $F(x_i)$ of the dLE2 compare much better to the MD data than the dLE1 results, which are found to significantly underestimate the barrier heights. While the achirality of Aib results in symmetric curves [i.e., $F(x_i) = F(-x_i)$], the observed asymmetry indicates insufficient sampling of the slow dynamics for the 16 μs time of the MD simulation.

As a further characterization of the structural dynamics of Aib_9, we next consider a Markov state model [2,24,25] that describes the metastable conformational states by a product state of right-handed (r) and left-handed (l) residues [12]. Restricting ourselves to the five inner

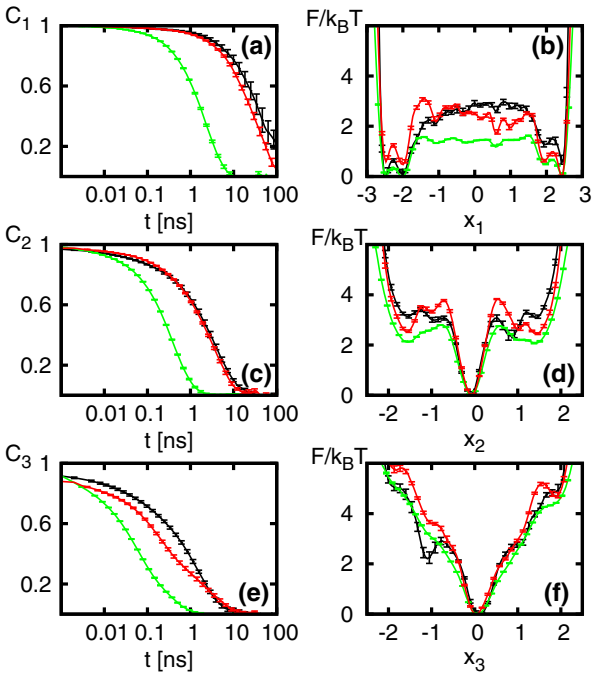

FIG. 2 (color online). Autocorrelation functions (panels a, c and e) and free energy curves (in units of $k_B T$, panels b, d and f) of the first three PCs of Aib_9. Compared are the MD reference data (black) and the dLE2 (red) and dLE1 (green) results. The bars account for the standard error.

residues of Aib_9, we obtain, e.g., $L = (lllll)$ and $R = (rrrrr)$, as well as $(rllll)$ if all but residue 3 show left-handed conformations. The definition facilitates a network representation of the global energy landscape [Fig. 3(a)], which reveals all possible pathways of the $L \leftrightarrow R$ transition of Aib_9. The network is defined by a transition matrix $\{T_{ij}\}$, where T_{ij} represents the probability of a state i to change to state j within a predefined lag time ($\tau = 1$ ns) and the self-transition probability T_{ii} represents the metastability of state i [2]. Considering the metastabilities of the main states and their transition probabilities, Fig. 3 shows a convincing agreement between the reference MD simulations and the dLE2 model, while the dLE1 performs significantly more weakly.

To explain the origin of this breakdown of the dLE1 model, Fig. 4(a) shows the acceleration $\ddot{x}_1$ as obtained from the MD simulations. When we represent $\ddot{x}_1$ in units of the average force $\langle f_1 \rangle \equiv -\langle \partial F / \partial x_1 \rangle$, we find that the acceleration is not negligible as assumed in the dLE1. Comparing $\ddot{x}_1$ to the corresponding free energy curve $F(x_1)$, it is seen that the acceleration tends to stabilize the system by pushing it back to the closest energy minimum. For example, for the minimum of $F(x_1)$ at $x_1 = -1.9$, we find for $x_1 \leq -1.9$ a positive value of $\ddot{x}_1$ and for $x_1 \geq -1.9$ a negative value of $\ddot{x}_1$, which both direct the system back to the minimum. This effect (which is completely neglected by the dLE1) appears to explain the

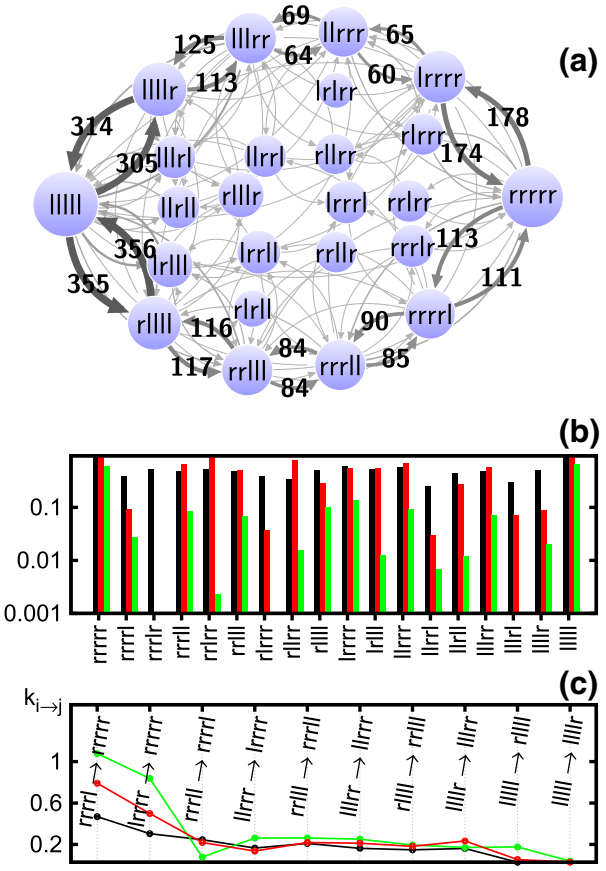

FIG. 3 (color online). (a) Network representation of the free energy landscape of Aib_9, illustrating the pathways of the conformational transitions leading from $L = (lllll)$ to $R = (rrrrr)$ and back. The size of the major nodes reflects their population and the size of the arrows accounts for the associated transition probabilities. For a few representative states the numbers of transitions are given. (b) Comparison of MD (black), dLE1 (green), and dLE2 (red) results for the metastabilities of the main states. (c) Same comparison for the transition probabilities.

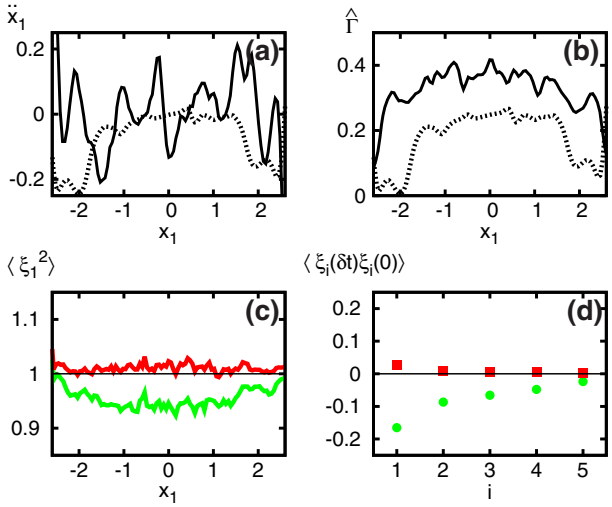

FIG. 4 (color online). Top: MD results for (a) the acceleration $\ddot{x}_1$ (in units of the average force $\langle f_1 \rangle$) and (b) friction tensor element $\hat{\Gamma}_{11}$ ($0 \le \hat{\Gamma}_{ij} \le 1$) as a function of x_1 (black lines). For comparison the free energy curve $F(x_1)$ (in arbitrary units) is shown as a dashed line. Bottom: properties of the noise $\xi_i(t)$ obtained from the dLE1 (green circles) and the dLE2 (red squares). Shown are (c) the variance $\langle \xi_1^2 \rangle$ as a function of x_1 and (d) the initial decay of the autocorrelation function at the first time step δt (i.e., $\langle \xi_i(\delta t)\xi_i(0) \rangle$) for all system coordinates x_i ($i = 1, \ldots, 5$).

too low energy barriers and too short autocorrelation decay times recovered by the dLE1 (Fig. 2). As a second example, Fig. 4(b) shows the dLE2 results of element $\hat{\Gamma}_{11}$ of the friction tensor $\hat{\Gamma} = \Gamma - \mathbb{I}$. While $\hat{\Gamma}_{ij} \equiv 0$ for overdamped motion [cf. Eq. (3)], Fig. 4(b) clearly exhibits nonzero friction, in particular in regions of high free energy.

Apart from improving the results of the dLE1, more importantly, the dLE2 represents a conceptional innovation. This becomes evident when we consider the properties of the noise, which in the derivation of both the dLE1 and the dLE2 were assumed to be of zero mean, unit variance, and delta correlated. [As described in Ref. [13], the noise trajectory $\xi_i(t)$ of the ith system coordinate can be back calculated by requiring that the dLE reproduce the original data at every time step.] Both approaches give zero mean, $\langle \xi_i \rangle \approx 0$ (data not shown). On the other hand, Fig. 4(c) reveals that the resulting variance of the noise $\langle \xi_1^2 \rangle$ is significantly too low for the dLE1, while the dLE2 nicely exhibits unit variance. Considering the associated noise autocorrelation functions $\langle \xi_i(t)\xi_i(0) \rangle$, we note that only the zeroth ($t = 0$) and first ($t = \delta t$) time point are of relevance for a memory-free (i.e., Markovian) Langevin equation. Since initially $\langle \xi_i(0)\xi_i(0) \rangle = 1$, we only need to consider the first decay to $\langle \xi_i(\delta t)\xi_i(0) \rangle$, see Fig. 4(d). We find nonzero results for the dLE1, which reflect significant memory of the noise and suggest that the dLE1 is not an appropriate model. The nonadequacy of the dLE1 model also becomes evident when we recall that equilibrium properties such as the free energy landscape are independent of the kinetic part of the Hamiltonian and therefore should not be affected by inertial effects (but see Fig. 2). On the other hand, the noise of the dLE2 is virtually delta correlated. Satisfying all assumptions made in its derivation, the dLE2 therefore represents a consistent and correct dynamical model of the considered data.

There are more conceptional virtues of a dLE2 model, even if the dynamics is overdamped. First, we wish to stress that the dLE2 contains well-established physical observables such as a Newtonian force term $\boldsymbol{f}(\boldsymbol{x}) = -\nabla F(\boldsymbol{x})$, a Stokes' friction term $\Gamma(\boldsymbol{x})\dot{\boldsymbol{x}}$, and a stochastic force $\mathcal{K}(\boldsymbol{x})\boldsymbol{\xi}(t)$, which can be readily employed for a further analysis or modeling of the system. In contrast, the direct interpretation of the dLE1 fields is less obvious. For example, the drift field in Eq. (1) is given by $\boldsymbol{h}(\boldsymbol{x}) = -\Gamma^{-1}\nabla F(\boldsymbol{x}) + k_B T \boldsymbol{I}(\boldsymbol{x})$, where $\boldsymbol{I}(\boldsymbol{x})$ is an additional noise-induced drift term that reflects the particular realization of

the stochastic integration, e.g., if Ito's or Stratonovich's method is employed [26]. In some sense the dLE1 fields therefore appear more as a fit of the data, while the dLE2 constitutes a more physical model. Lastly, we wish to mention that the dLE2 also suggests a simple enhanced sampling method, which exploits the fact that the dLE2 contains the temperature as a driving force. Using the fluctuation-dissipation theorem, one can run a high-temperature simulation to calculate the Langevin fields, and subsequently use these fields to perform a dLE2 simulation at the desired temperature [27].

To summarize, we have demonstrated that small damping effects can be important to correctly describe the statistics (e.g., the energy landscape) and dynamics (e.g., the corresponding autocorrelation function) of biomolecular systems. To include these effects in a dynamical model, we have derived an algorithm that propagates a second-order Langevin scheme (dLE2), which facilitates the treatment of multidimensional data. Adopting extensive MD simulations of a peptide helix and employing dihedral angle PCA, we have constructed a five-dimensional dLE2 model to forecast the complex structural dynamics of the solvated biomolecule. The model has been shown to well reproduce all quantities of interest, including the results of a previously devised Markov state model. Much more than being a mere improvement of the overdamped Langevin equation, the dLE2 provides a consistent and correct description of the dynamics, as it satisfies the underlying assumptions of the dynamical model.

The dLE program can be obtained by following the link in Ref. [28].

We thank Andrzej Rzepiela and Sebastian Buchenberg for numerous instructive and helpful discussions. This work has been supported in part by the Deutsche Forschungsgemeinschaft.

*stock@physik.uni-freiburg.de

[1] H. Kantz and T. Schreiber, *Nonlinear Time Series Analysis* (Cambridge University Press, Cambridge, England, 1997).
[2] G. R. Bowman, V. S. Pande, and F. Noe, *An Introduction to Markov State Models* (Springer, Heidelberg, 2013).
[3] W. T. Coffey and Y. P. Kalmykov, *The Langevin Equation* (World Scientific, Singapore, 2012).
[4] O. F. Lange and H. Grubmüller, Collective Langevin dynamics of conformational motions in proteins, J. Chem. Phys. **124**, 214903 (2006).
[5] J. Gradišek, S. Siegert, R. Friedrich, and I. Grabec, Analysis of time series from stochastic processes, Phys. Rev. E **62**, 3146 (2000).
[6] J. Timmer, Parameter estimation in nonlinear stochastic differential equations, Chaos, Solitons and Fractals **11**, 2571 (2000).
[7] G. Hummer, Position-dependent diffusion coefficients and free energies from Bayesian analysis of equilibrium and replica molecular dynamics simulations, New J. Phys. **7**, 34 (2005).
[8] C. Micheletti, G. Bussi, and A. Laio, Optimal Langevin modeling of out-of-equilibrium molecular dynamics simulations , J. Chem. Phys. **129**, 074105 (2008).
[9] R. Hegger and G. Stock, Multidimensional Langevin modeling of biomolecular dynamics , J. Chem. Phys. **130**, 034106 (2009).
[10] A. J. Rzepiela, N. Schaudinnus, S. Buchenberg, R. Hegger, and G. Stock, Communication: Microsecond peptide dynamics from nanosecond trajectories: A Langevin approach, J. Chem. Phys. **141**, 241102 (2014).
[11] R. Zwanzig, *Nonequilibrium Statistical Mechanics* (Oxford University, Oxford, 2001).
[12] S. Buchenberg, N. Schaudinnus, and G. Stock, Hierarchical biomolecular dynamics: Picosecond hydrogen bonding regulates microsecond conformational transitions, J. Chem. Theory Comput. **11**, 1330 (2015).
[13] N. Schaudinnus, A. J. Rzepiela, R. Hegger, and G. Stock, Data driven Langevin modeling of biomolecular dynamics , J. Chem. Phys. **138**, 204106 (2013).
[14] H. Frauenfelder, S. Sligar, and P. Wolynes, The energy landscapes and motions of proteins, Science **254**, 1598 (1991).
[15] J. N. Onuchic, Z. L. Schulten, and P. G. Wolynes, Theory of protein folding: The energy landscape perspective, Annu. Rev. Phys. Chem. **48**, 545 (1997).
[16] K. A. Dill and H. S. Chan, From levinthal to pathways to funnels: The "New View" of protein folding kinetics, Nat. Struct. Biol. **4**, 10 (1997).
[17] D. J. Wales, *Energy Landscapes* (Cambridge University Press, Cambridge, England, 2003).
[18] D. van der Spoel, E. Lindahl, B. Hess, G. Groenhof, A. E. Mark, and H. J. C. Berendsen, Gromacs: Fast, flexible, and free, J. Comput. Chem. **26**, 1701 (2005).
[19] T. Ichiye and M. Karplus, Collective motions in proteins: A covariance analysis of atomic fluctuations in molecular dynamics and normal mode simulations, Proteins **11**, 205 (1991).
[20] A. E. Garcia, Large-Amplitude Nonlinear Motions in Proteins, Phys. Rev. Lett. **68**, 2696 (1992).
[21] A. Amadei, A. B. M. Linssen, and H. J. C. Berendsen, Essential dynamics of proteins, Proteins **17**, 412 (1993).
[22] B. L. de Groot, X. Daura, A. E. Mark, and H. Grub-müller, Essential dynamics of reversible peptide folding: memory-free conformational dynamics governed by internal hydrogen bonds, J. Mol. Biol. **309**, 299 (2001).
[23] A. Altis, P. H. Nguyen, R. Hegger, and G. Stock, Dihedral angle principal component analysis of molecular dynamics simulations, J. Chem. Phys. **126**, 244111 (2007).
[24] K. A. Beauchamp, G. R. Bowman, T. J. Lane, L. Maibaum, I. S. Haque, and V. S. Pande, MSMBuilder2: Modeling conformational dynamics on the picosecond to millisecond scale, J. Chem. Theory Comput. **7**, 3412 (2011).
[25] J.-H. Prinz, H. Wu, M. Sarich, B. Keller, M. Senne, M. Held, J. D. Chodera, C. Schütt, and F. Noé, Markov models of molecular kinetics: Generation and validation, J. Chem. Phys. **134**, 174105 (2011).
[26] H. Risken, *The Fokker-Planck Equation* (Springer, Berlin, 1989).
[27] N. Schaudinnus, B. Bastian, R. Hegger, and G. Stock (to be published).
[28] http://www.theochem.uni-frankfurt.de/~hegger/langevin.tar.gz